Causes and consequences of pronounced variation in the isotope composition of plant xylem water

Hannes P.T. De Deurwaerder [(1,2)*], Marco D. Visser [(2)], Matteo Detto [(2)], Pascal Boeckx [(3)], Félicien Meunier [(1,4)], Kathrin Kuehnhammer [(5,6)], Ruth-Kristina Magh [(7,8)], John D. Marshall [(8)], Lixin Wang [(9)], Liangju Zhao [(10,11)], Hans Verbeeck [(1)]

(1) CAVElab - Computational & Applied Vegetation Ecology, Faculty of Bioscience Engineering, Ghent University, Ghent, Belgium

(2) Department of Ecology and Evolutionary Biology, Princeton University, Princeton, NJ, USA

(3) ISOFYS – Isotope Bioscience Laboratory, Faculty of Bioscience Engineering, Ghent University, Ghent, Belgium

(4) Ecological Forecasting Lab, Department of Earth and Environment, Boston University, Boston, Massachusetts, USA

(5) IGOE, Umweltgeochemie, Technische Universität Braunschweig, Braunschweig, Germany

(6) Ecosystem Physiology, University of Freiburg, Freiburg, Germany,

(7) Institute for Forest Sciences, Chair of Tree Physiology, University of Freiburg, Freiburg, Germany

(8) Department of Forest Ecology and Management, SLU, Swedish University of Agricultural Sciences, Umeå, Sweden

(9) Department of Earth Sciences, Indiana University-Purdue University Indianapolis (IUPUI), Indianapolis, IN 46202, USA

(10) Shaanxi Key Laboratory of Earth Surface System and Environmental Carrying Capacity, College of Urban and Environmental Sciences, Northwest University, Xi'an 710127, China

(11) Key Laboratory of Ecohydrology and Integrated River Basin Science, Northwest Institute of Eco-Environment and Resources, Chinese Academy of Sciences, Lanzhou 730000, China

*Correspondence to: Hannes De Deurwaerder (Hannes_de_deurwaerder@hotmail.com)

Abstract

1. Stable isotopologues of water are widely used to derive relative root water uptake (RWU) profiles and average RWU depth in lignified plants. Uniform isotope composition of plant xylem water (δ_{xyl}) along the stem length of woody plants is a central assumption of the isotope tracing approach, which has never been properly evaluated.

2. Here we evaluate whether strong variation in δ_{xyl} within woody plants exists using empirical field observations from French Guiana, northwestern China, and Germany. In addition, supported by a mechanistic plant hydraulic model, we test hypotheses on how variation in δ_{xyl} can develop through the effects of diurnal variation in RWU, sap flux density, diffusion, and various other soil and plant parameters on the δ_{xyl} of woody plants.

3. The hydrogen and oxygen isotope composition of plant xylem water shows strong temporal (i.e., sub-daily) and spatial (i.e., along the stem) variation ranging up to 25.2‰ and 6.8‰ for δ^2H and $\delta^{18}O$ respectively, greatly exceeding measurement error range in all evaluated datasets. Model explorations predict that significant δ_{xyl} variation could arise from diurnal RWU fluctuations and vertical soil water heterogeneity. Moreover, significant differences in δ_{xyl} emerge between individuals that differ only in sap flux densities, or are monitored at different times or heights.

4. This work shows a complex pattern of δ_{xyl} transport in the soil-root-xylem system, which can be related to the dynamics of RWU by plants. These dynamics complicate the assessment of RWU when using stable water isotopologues, but also open new opportunities to study drought responses to environmental drivers. We propose to include monitoring of sap flow and soil matric potential for more robust estimates of

52   average RWU depth and expansion of attainable insights in plant drought strategies and

53   responses.

54

Keywords

56   Ecohydrology, Lianas, Root water uptake, Sap flow, Stable isotope composition of water,

57   Tropical trees, Water competition

58

1. Introduction

The use of stable isotope composition of water has strengthened ecohydrology studies by providing insights into phenomena that are otherwise challenging to observe, such as relative root water uptake depth (RWU depth) (Rothfuss & Javaux, 2017), below-ground water competition and hydraulic lift (Hervé-Fernández *et al.*, 2016; Meunier *et al.*, 2017). Compared to root excavation, the technique is far less destructive and labor-intensive. This makes it more flexible for studying multiple individuals across spatial and temporal scales (i.e. individual to ecosystem, daily to seasonal) (Dawson *et al.* 2002). Besides, the study of stable isotope composition of xylem water measures the real effects of RWU at different depths whereas excavation yields only root distribution and architecture. The advantages and wide applicability of this method make it a popular technique that pushes the boundaries of ecohydrology (Dawson *et al.*, 2002; Yang *et al.*, 2010; Rothfuss & Javaux, 2017; Lanning *et al.*, 2020)

A variety of methods are used to infer average RWU depth from the isotope composition of plant xylem water (δ_{xyl}), but all rely on a direct relationship between the isotopic compositions of plant xylem and soil water (Ehleringer & Dawson, 1992). All have two key assumptions. The first is that the isotope composition of plant xylem water remains unchanged during transport from root uptake to evaporative sites (e.g. leaves and non-lignified green branches). Hence, isotopic fractionation – i.e. processes that cause a shift in the relative abundances of the water isotopologues, driven by their differences in molecular mass – do not occur during the transport from the uptake to the evaporative site (Wershaw *et al.*, 1966; Zimmermann *et al.*, 1967; White *et al.*, 1985; Dawson & Ehleringer, 1991; Walker & Richardson, 1991; Dawson *et al.*, 2002; Zhao *et al.*, 2016). Second, all methods assume that xylem water provides a well-mixed isotope composition of water from different soil layers: sampled xylem water instantaneously reflects the distribution and water uptake of the roots independent of the timing or height of sampling.

84 The first assumption is relatively well supported. Isotopic fractionation at root level does

85 not raise concerns for most RWU assessments using water isotopologues (Rothfuss & Javaux,

86 2017) except for kinetic fractionation that might occur during water transported across the root

87 membrane in extreme environments (Lin & Sternberg, 1993; Ellsworth and Williams, 2007;

88 Zhao *et al.*, 2016). Similarly, isotopic fractionation of water within an individual plant, although

89 possible, is generally not considered a serious problem (Yakir, 1992; Dawson & Ehleringer,

90 1993; Cernusak *et al.*, 2005; Mamonov *et al.*, 2007; Zhao *et al.*, 2016). This perception was

91 recently contested by Barbeta *et al* (2020), advocating a more general nature of the occurrence

92 of isotopic offsets between xylem water and potential water sources. As the origin of these

93 offsets remains debated, future research should clarify its impact on the applicability of stable

94 water isotopic compositions for RWU assessment. However, the second assumption of time

95 and space invariance of the isotope composition of xylem water has, to our knowledge, never

96 been assessed.

97 Various plant physiological processes, ranging from very simple to more complex

98 mechanisms, could influence within plant variation in δ_{xyl} at short time scales, i.e. sub-daily to

99 sub-hourly. For instance, plant transpiration during the day is regulated by stomata according

100 to water supply and atmospheric demand, and follows well known diurnal patterns (Steppe &

101 Lemeur, 2004; Epila *et al.*, 2017). This results in a changing water potential gradient between

102 soil and leaves throughout the day (Fig 1a,b), which in turn affects the depth of the average

103 RWU (Goldstein *et al.*, 1998; Doussan *et al.*, 2006; Huang *et al.*, 2017). Hence, shifts in a

104 plant's capacity to take up water at different soil layers during the day can generate diurnal

105 variation in the mixture of isotope composition from water taken up from various depths (Fig

106 1c). Subsequently, this water mixture moves up along the xylem with the velocity of the sap

107 flux density. As these sap flux densities depend on species and individual-specific hydraulic

108 traits and their responses to atmospheric water demand and soil moisture availability, complex

109 dynamics in isotopic composition will emerge and propagate through the plant. The above

110 hypothesis, if true, would make the comparison of isotopic data among individuals, species,

111 and studies difficult.

112   In this study, we provide a critical assessment of the assumption of δ_{xyl} invariance along

113 the length of woody plant stems and over short time periods. We first show that variation in δ_{xyl}

114 along the length of lignified plants exceeds the expected measurement error using three

115 independent datasets including i) canopy trees and lianas sampled at different heights in French

116 Guiana; and ii) plant species from northwestern China (Zhao *et al.*, 2014) and iii) European

117 Beech and Silver firs in south-west Germany (Magh *et al.*, 2020). Second, we build a simple

118 mechanistic model that incorporates basic plant hydraulic transport processes. The model

119 predicts that diurnal changes in water potential gradient between soil and roots result in shifting

120 sources of water absorption that differ in their isotope composition.

121

2. Materials and Methods

2.1. Part A: Empirical exploration

2.1.1. Field data French Guiana: variation in δ_{xyl} with plant height

125 Six canopy trees and six canopy lianas were sampled during two subsequent dry days (24-25

126 August 2017) at the Laussat Conservation Area in Northwestern French Guiana (05°28.604'N-

127 053°34.250'W). Stem xylem tissue of individual plants was sampled at different heights (1.3,

128 5, 10, 15 and 20 m where possible) at the same radial position of the stem, between 9:00 and

129 15:00. Stem samples were stripped off bark and phloem tissues. Soil samples were collected at

130 different depths (0.05, 0.15, 0.30, 0.45, 0.60, 0.90, 1.20, and 1.80m) with a soil auger and in

131 close vicinity to the sampled individuals. Samples were placed in glass collection vials, sealed

132 with a cap, and frozen awaiting cryogenic vacuum distillation (CVD; 4 h at 105°C). When the

133   weight loss of a sample resulting from the extraction process was below 98%, the sample was

134   excluded (after Araguás-Araguás *et al.*, 1998) (see Fig S1).

135   The isotope composition of the water in the samples was measured with a Wavelength-

136   Scanned-Cavity Ring-Down Spectrometer (WS-CRDS, L2120-i, Picarro, California, USA)

137   coupled with a vaporizing module (A0211 High Precision Vaporizer) and a micro combustion

138   module to avoid organic contamination (Martin-Gomez et al., 2015; Evaristo et al., 2016). Post-

139   processing of raw δ-readings into calibrated δ-values (in ‰, V-SMOW) was performed using

140   SICalib (version 2.16; Gröning, 2011). More details on the sampling site and sampling

141   procedure can be found in supplementary methods A.

142   **2.1.2.   Field data China: temporal variation in δ_{xyl}**

143   Plant δ_{xyl} was sampled at high temporal resolution in the Heihe River Basin (HRB),

144   northwestern China. Four distinct study locations differing in altitude, climatological

145   conditions, and ecosystem types were selected. At each location, the dominant tree, shrub,

146   and/or herb species were considered for sampling. In August 2009, *Populus euphratica* was

147   sampled in the Qidaoqiao riparian forest (42°01'N-101°14'E) and *Reaumuria soongorica* in the

148   Gobi desert ecosystem (42°16'N-101°17'E; 906-930 m a.s.l). In June–September 2011 *Picea*

149   *crassifolia*, *Potentilla fruticose, Polygonum viviparum* and *Stipa capillata* were measured in

150   the Pailugou forest ecosystem (38°33'N-100°18'E; 2700-2900 m a.s.l). All species were

151   sampled every 2-hours over multiple days (3-4), except for *P. crassifolia,* which was measured

152   hourly. Stem samples were collected for trees and shrubs, while root samples were obtained for

153   the herb species. More details are available in Zhao *et al.* (2014).

154   Upon collection, all samples were placed in 8 mL collection bottles and frozen in the

155   field stations before transportation to the laboratory for water extraction via CVD (Zhao *et al.*,

156   2011). Both $\delta^{18}O$ and δ^2H were assessed with an Euro EA3000 element analyzer (Eurovector,

157   Milan, Italy) coupled to an Isoprime isotope ratio mass spectrometer (Isoprime Ltd, UK) at the

158   Heihe Key Laboratory of Ecohydrology and River Basin Science, Cold and Arid Regions

159   Environmental and Engineering Research Institute. Internal laboratory references were used for

160   calibration, resulting in measurement precision of ±0.2‰ and ±1.0 ‰ for $\delta^{18}O$ and $\delta^{2}H$,

161   respectively.

2.1.3. Field data Germany: high temporal variation in δ_{xyl}

163   A δ_{xyl} monitoring campaign, studying mature Silver firs (*Abies alba*; n=3) and European

164   beeches (*Fagus sylvatica*; n=3), was conducted during progressing drought conditions (6-11

165   July 2017) at the "Freiamt" field site in south-west Germany. Isotopic composition of xylem

166   water was obtained from branch samples, which were collected every two hours between 7:00

167   and 21:00 at the same height and canopy orientation in the sun crown. Branches were stripped

168   of bark and phloem tissue. A Scholander Pressure chamber (Scholander, 1966), which allowed

169   concomitant registration of water potential of the sampled branches, was used to extract xylem

170   water directly in the field (Rennenberg *et al.*, 1996). Both $\delta^{18}O$ and $\delta^{2}H$ of branch samples were

171   determined with a wavelength scanned cavity ring-down spectrometer (Picarro L2130i, Santa

172   Clara, USA), followed by data correction using ChemCorrect^{TM} (Picarro, 2010). For more

173   details see Magh *et al.* (2020).

174

2.1.4. Field data normalization

176   To aid visual comparisons, we use normalized δ_{xyl} values ($\beta^{2}H_X$ and $\beta^{18}O_X$) which describe

177   the deviation of an individual sample from the average isotopic composition (a) along the height

178   *h* of the stem, or (b) over one day:

$$\beta^{2}H_X = \delta^{2}H_X - \frac{1}{N}\sum_{j=1}^{N}\delta^{2}H_{X,j} \qquad\qquad \text{Eq. (1)}$$

180   With *N* the number of sampled heights or time steps during one day.

181

2.2. Part B: Model exploration

2.2.1. Model derivation

The expected δ_{xyl} at different stem heights within a tree during the course of the day can be

derived from plant and physical properties such as root length density, total fine root surface

area, water potential gradients, and the isotope composition of soil water (Fig. 2). We call this

the SWIFT model (i.e. Stable Water Isotopic Fluctuation within Trees). To derive the SWIFT

model, we first describe the establishment of δ_{xyl} entering the tree at the stem base via a multi-

source mixing model (Phillips & Gregg, 2003). We subsequently consider vertical water

transport within the tree, which relates to the established sap flow pattern.

To ensure consistency and clarity in variable declarations we maintain the following

notation in the subscripts of variables: uppercase roman to distinguish the medium through

which water travels (X for xylem, R for root, S for soil) and lowercase for units of time and

distance (h for stem height, t for time and i for soil layer index). A comprehensive list of

variables, definitions, and units is given in Table 1. A schematic representation of the model is

provided in Fig. 2a. Note that the model presented here focuses on hydrogen isotopes (i.e.

^{2}H/^{1}H) but can easily be used to study oxygen isotopes (i.e. ^{18}O/^{16}O).

i.   Isotope composition of plant xylem water at stem base.

The δ^2H composition of xylem water of an individual plant at stem base ($\delta^2H_{X,0,t}$) (i.e.

height zero; $h = 0$m; Fig. 2a) at time t, can theoretically be derived by calculating a weighted

average of water taken up from different soil depths (Phillips & Gregg, 2003). The root zone is

divided into n discrete soil layers of equivalent thickness Δz. Here, we assume a constant δ^2H

composition of soil water ($\delta^2H_{S,i}$) over time in each soil layer, a reasonable assumption when

204   isotopic measurements are conducted during rain-free periods, allowing the expression of

205    $\delta^2 H_{X,0,t}$ as:

206    $$\delta^2 H_{X,0,t} = \sum_{i=1}^{n} f_{i,t} \cdot \delta^2 H_{S,i}$$ Eq. (2)

207   where $f_{i,t}$ is the fraction of water taken up at the ith soil layer (Fig. 2a) defined as:

208    $$f_{i,t} = \frac{RWU_{i,t}}{\sum_{i=1}^{n} RWU_{i,t}}$$ Eq. (3)

209   and $RWU_{i,t}$ is the net amount of water entering and leaving the roots at time t in the ith soil layer

210   ($RWU_{i,t}$ is defined positive when entering the root). The current representation of the model

211   does not account for water loss via the root system nor for mixing of the extracted water from

212   different soil layers within the roots until the water enters the stem base. When tree capacitance

213   is neglected, the sum of $RWU_{i,t}$ across the entire root zone is equal to the instantaneous sap

214   flow at time t, SF_t:

215    $$SF_t = \sum_{i=1}^{n} RWU_{i,t} = \sum_{i=1}^{n} -k_i \cdot A_{R,i} \cdot \left[\Psi_{X,0,t} - (\Psi_{S,i,t} - z_i) \right]$$ Eq. (4)

216   Where k_i is the plant-specific total soil-to-root conductance over soil layer i, $\Psi_{X,0,t}$ is the water

217   potential (i.e. the hydraulic head) at the base of the plant stem and $\Psi_{S,i,t}$ is the soil matric

218   potential at the ith soil layer (Fig. 2a). Total plant water potential is generally defined as the sum

219   of the solute, pressure, gravity, and matric potential. As long-distance water transport through

220   the xylem is studied, the osmotic potential and the kinetic energy head can be assumed

221   negligible (Früh & Kurth, 1999). The xylem pressure potential is represented as $\Psi_{X,0,t}$. And the

222   term z_i is the gravimetric water potential necessary to lift the water from depth z_i to the base of

223   the stem, assuming a hydrostatic gradient in the transporting roots. The model considers z_i to

224   be a positive value (zero at the surface), thus z_i is subtracted $\Psi_{S,i,t}$. $A_{R,i}$ is the absorptive root

225   area distribution over soil layer i (Fig. 2a). This parameter $A_{R,i}$ can be derived from plant

226   allometric relations with stem diameter (Čermák *et al.*, 2006), and subsequently distributed over

227   the different soil layers, considering the power-law distribution of Jackson *et al.* (1995).

228   The total soil-to-root conductance is calculated assuming the root and soil resistances are

229   connected in series (Fig. 2a):

230            $k_i = \frac{k_R \cdot k_S}{k_R + k_S}$ Eq. (5)

231   where k_R is the effective root radial conductivity (assumed constant and uniform), and $k_S =$

232      $K_{S,i}/\ell$ is the conductance associated with the radial water flow between soil and root surface.

233      $\ell = 0.53/\sqrt{\pi \cdot B_i}$ represents the effective radial pathway length of water flow between bulk soil

234   and root surface (De Jong van Lier *et al.*, 2008; Vogel *et al.*, 2013) with B_i giving the overall

235   root length density distribution per unit of soil. $K_{S,i}$ is the soil hydraulic conductivity for each

236   soil depth. $K_{S,i}$ depends on soil water moisture and thus relates to the soil matric potential $\Psi_{S,i,t}$

237   of the soil layer where the water is extracted. $K_{S,i}$ is computed using the Clapp & Hornberger

238   (1978) formulation:

239            $K_{S,i} = K_{s,max} \cdot \left(\frac{\Psi_{sat}}{\Psi_{S,i,t}}\right)^{2+\frac{3}{b}}$ Eq. (6)

240   where $K_{s,max}$ is the soil conductivity at saturation and b and Ψ_{sat} are empirical constants that

241   depend on soil type (here considered as constant over all soil layers).

242   Subsequently, $f_{i,t}$ can be restructured as:

243            $f_{i,t} = \frac{k_i \cdot A_{R,i} \cdot \Delta\Psi_{i,t}}{\sum_{i=1}^{n} k_i \cdot A_{R,i} \cdot \Delta\Psi_{i,t}}$ Eq. (7)

244   where the root water to soil matric potential gradient is represented as $\Delta\Psi_{i,t} = \Psi_{X,0,t} -$

245      $(\Psi_{S,i,t} - z_i)$.

246   Combining Eq. (2) and Eq. (7) then allows the derivation of $\delta^2 H_{X,0,t}$ as follows:

247
$$\delta^2 H_{X,0,t} = \sum_{i=1}^{n} \left(\frac{k_i \cdot A_{R,i} \cdot \Delta\Psi_{i,t}}{\sum_{j=1}^{n} k_j \cdot A_{R,j} \cdot \Delta\Psi_{j,t}} \cdot \delta^2 H_{S,i} \right)$$
Eq. (8)

248 This equation requires estimates of $\Delta\Psi_{i,t}$, which is preferably measured instantaneously in the

249 field (i.e. via stem and soil psychrometers for $\Psi_{X,0,t}$ and $\Psi_{S,i,t}$, respectively). However, as

250 measurements of $\Psi_{X,0,t}$ are not always available, estimated $\widehat{\Psi}_{X,0,t}$ can be derived from sap flow

251 by re-organizing Eq. (4) into:

252
$$\widehat{\Psi}_{X,0,t} = \frac{\sum_{i=1}^{n} [k_i \cdot A_{R,i} \cdot (\Psi_{S,i,t} - z_i)] - SF_t}{\sum_{i=1}^{n} k_i \cdot A_{R,i}}$$
Eq. (9)

253 which then allows replacement of $\Psi_{X,0,t}$ with $\widehat{\Psi}_{X,0,t}$ in Eq. (8).

254  *ii. Height-dependent isotope composition of plant xylem water*

255  In our model, the water isotopologues simply move upwards from the stem base with

256 the sap flow velocity. Assuming negligible diffusion, the δ^2H isotope composition in xylem

257 water at height h and time t ($\delta^2 H_{X,h,t}$) is then the isotope composition of xylem water at stem

258 base at time $t - \tau$.

259
$$\delta^2 H_{X,h,t} = \delta^2 H_{X,0,t-\tau}$$
Eq. (10)

260 where τ is the lag before $\delta^2 H_{X,0,t}$ reaches stem height h (Fig. 2a), which depends on the true

261 sap flux density in the xylem (SF_V). True sap flux density indicates the real speed of vertical

262 water displacement within a plant, derived by dividing SF_t over the lumen area of the plant (A_x;

263 Fig. 2a) i.e. the total cross-sectional area of the vessels. τ can be obtained from the mass

264 conservation equality:

265
$$h \cdot A_x = \int_{t-\tau}^{t} SF_t \, dt$$
Eq. (11)

266   Note that since most scientific studies express sap flux density as the sap flow over the total

267   sapwood area (SF_S), rather than over the total vessel lumen area (SF_V), for consistency, we will

268   present the model outputs as functions of SF_S.

269   Note that SF_V presents the sap flux density normalized over the total vessel lumen area, and

270   as vessel lumen area correlates with plant diameter at breast height (DBH), there is no need for

271   explicit consideration of DBH in the model for comparison among field measurements.

272   Model analyses show that the impact of the mutual diffusion coefficient of heavy water in

273   normal water on the transport flux is negligible for plants with high sap flux densities, which is

274   the case for the theoretical examples below. However, in plants with low sap flow densities,

275   consideration of diffusion might be required. Diffusion might also be generated by water

276   passing through a complex network of vessels, in analogy to diffusion in a porous media (see

277   supplementary methods B for some analytical results, simulated cases of and a detailed

278   discussion on the role of diffusion). SWIFT was implemented in R version 3.4.0 (R Core Team,

279   2017), and is publicly available (see GitHub repository HannesDeDeurwaerder/SWIFT).

280   *iii.   Model parameterization and analyses*

281   The model's primary purpose is to gain insight into 1) which processes are capable of

282   generating δ_{xyl} variance, and 2) how sensitive the variance in δ_{xyl} along the stem is in response

283   to the modeled plant hydraulic processes. To this end, we adopted the basic plant parameters

284   from Huang *et al.* (2017) who studied soil-plant hydrodynamics of loblolly pine (*Pinus taeda*

285   *L.*) during a 30-day extended dry down period (Table S1). We started with synthetic basal sap

286   flow patterns and volumes extracted from the model runs of Huang *et al.* (2017) for a typical

287   drought day (day 11). Both basal sap flow patterns and volumes are repeated over the studied

288   period, as no variation between days is assumed. Sap flow follows the plant's water demand

289   which is the result of daily cycles of transpiration driven by photosynthetic active solar radiation

290 (PAR), vapor pressure deficit (VPD), and optimal stomatal response (Epila *et al.*, 2017).

291 Secondly, both the soil matric potential ($\Psi_{S,i,t}$) and δ^2H composition of soil water ($\delta^2H_{S,i}$)

292 profiles with soil depth were adopted from Meißner *et al.* (2012) (Fig. S8, see Table S1 for

293 equations) as driver data of the model, and were assumed to stay constant over time. Since

294 measurements of Meißner *et al.* (2012) were conducted at a silt loam plot in the temperate

295 climate of central Germany, corresponding soil parameters were selected from Clapp &

296 Hornberger (1978). Subsequently, the following model simulations were executed (see Fig. 2a):

297   1) **Analysis A1: impact of temporal SF$_t$ variation on the isotope composition of**

298   **xylem water at a fixed stem height.** Temporal patterns in δ^2H isotope composition

299   in xylem water (δ^2H_X) were evaluated for a typical situation, i.e. measurement at

300   breast height (*h*=1.30 m) (e.g. White *et al.*, 1985; Meinzer *et al.*, 1999; Goldsmith

301   *et al.*, 2012; Hervé-Fernández *et al.*, 2016; De Deurwaerder *et al.*, 2018; Muñoz-

302   Villers *et al.*, 2019).

303   2) **Analysis A2: impact of temporal SF$_t$ variation at different tree heights.**

304   Temporal patterns in δ^2H_X within a tree at various sampling heights (5, 10, and 15

305   m).

306   3) **Analysis A3: impact of temporal SF$_t$ variation on the isotope composition of**

307   **xylem water and the timing of sampling.** Representation of the profile of δ^2H_X

308   along the full height of a tree, measured at different sampling times (9:00 and 11:00),

309   with the standard parameterization given in Table S1.

310   4) **Analysis B: variation in δ^2H_X due to differences in absolute daily average sap**

311   **flow speed.** Diurnal patterns in the δ^2H_X in trees that differ solely in daily averaged

312   SF_V, which are set to 0.64, 0.42, and 0.19 m h^{-1}, respectively corresponding to SF_S

313   values of 0.09, 0.06 and 0.03 m h^{-1}.

314   All parameters of the four analyses are given in Table S1. The model simulations

315   for each analysis were compared to a null model.

316

317   *iv.*   *The null model*

318   The null model adopts the standard assumption of zero variation in δ_{Xyl} along the length

319   of the plant body, but allows for potential measurement errors related to the extraction protocol.

320   In reality, empirically obtained data will have some variation as observed values $(Obs.\,\delta_{Xyl})$

321   are the sum of the true δ_{Xyl}-values and their extraction error $(error_{extraction})$.

322       $Obs.\,\delta_{Xyl} = True\ \delta_{Xyl} + error_{extraction}$ (eq. 12)

323   Hence, the null model attributes any variance in isotopic composition to extraction errors, with

324   maximum extraction error ranges of 3‰ for $\delta^2 H$ samples (0.3‰ for $\delta^{18} O$) expected for water

325   extraction recovery rates higher than 98% (e.g. Orlowski *et al.*, 2013). These extraction errors

326   are negatively skewed following the Rayleigh distillation model, which predicts that extraction

327   error for incomplete water recovery will be negative, and therefore Obs. δ_{xyl} ≤ True δ_{xyl}. The

328   null model represents this $error_{extraction}$ by a negative skew-normal distribution (with location

329   parameter ξ = 0‰, the scale ω = 3‰ for $\delta^2 H$ or 0.3‰ for $\delta^{18} O$, and shape α = -∞) (Azzalini,

330   2013).

331

332   **2.2.2. Estimation of average RWU depth**

333   Average RWU depths (i.e. the weighted mean of the depths of RWU, with the uptake fractions

334   at the different depths as weights) were derived from the simulated $\delta^2 H_X$ values by use of both

335   the direct inference method and the end-member mixing analysis method. Together, these

336   techniques represent 96% of the applied methods in the literature (Rothfuss & Javaux, 2017),

337   and the reader is referred to Rothfuss & Javaux (2017) for a complete discussion of both

techniques. In line with the general approach assessing RWU with stable water isotopes, the average RWU depth is obtained by relating the δ^2H_X with the $\delta^2H_{S,i}$ depth profile. We compared average RWU depth estimates obtained from simulated δ^2H_X, as described in the analyses above, with the true average RWU depth. Here, the true average RWU depth was defined as the depth corresponding to the daily weighted average δ^2H_X, calculated as the weighted sum of $\delta^2H_{X,i,t}$ and the relative fraction of water taken up at each depth.

2.2.3. Transport dynamics and sensitivity analysis

We perform a basic model validation of our model assumption that the propagation of an isotopic signature is driven by diurnal sap flow dynamics and diffusion alone. In essence, the model assumes that once water with a given isotopic signature enters the stem, it moves upwards with the speed of sap flow, and changes only due to the effect of diffusion. The effects of capacitance on δ^2H_X dynamics by the release of storage water in the xylem flow can be ignored. To validate this assumption we compare model predictions against observed δ^2H_X dynamics monitored within a pine tree (*Pinus pinea L.*) following [2]H-enrichment in a controlled greenhouse experiment, as detailed in Marshall *et al.* (2020). δ^2H_X was measured at two heights (0.15 and 0.65m) using a novel *in situ* technique, the borehole equilibration method. Performed model simulations consider the absolute ranges of sap flux densities during the entire monitoring campaign, with the account of tree tapering effect on sap flux densities over the studied stem length (supplementary method C). Validation of diurnal variation in δ^2H_X requires high temporal resolution monitoring of δ^2H_X dynamics in plants stems, with simultaneous high temporal resolution monitoring and characterization of sap flow, soil water potential, and isotopic composition. Such data does not yet exist to our best of knowledge.

In addition, we performed two sensitivity analyses to assess the relative importance of each parameter in generating variance in δ^2H_X along the length of a plant. In both sensitivity analyses,

363 we varied model parameters one-at-a-time to assess the local sensitivity of the model outputs

364 for soil type, sap flux density, root properties, and sampling strategies. The sensitivity analysis

365 provides insight into possibilities for improving the design of field protocols, by revealing

366 potential key measurements and caveats in field setups. More details on the performed

367 sensitivity analysis and validation of transport dynamics are available in supplementary method

368 C.

369

370 3. Results

371 3.1. Part A: Empirical exploration

372 The null model assumes constant isotopic composition of root water uptake, with only limited

373 variance in isotopic composition introduced by extraction errors ($\beta^2 H_X < 3‰$; $\delta^{18}O_X < 0.3‰$).

374 However, pronounced $\delta^2 H_X$ variance within individual plants, exceeding the null model ranges,

375 are observed in all three independent datasets. The normalized $\delta^2 H$ composition in xylem water

376 ($\beta^2 H_X$) along the stem length of lianas and trees in French Guiana exceeded the null model by

377 a factor of 3.2 and 4.3, respectively (Fig. 3c, Fig. S2). Differences up to 13.1‰ and 18.3‰ in

378 $\delta^2 H$ and 1.3‰ and 2.2‰ in $\delta^{18}O$ were observed in individuals of trees and lianas, respectively

379 (Supplementary method A, table A,).

380 Similarly, diurnal intra-individual $\delta^2 H_X$ variances were found for all considered plant

381 growth forms, i.e. trees, shrubs, and herbs, monitored in China (Fig. 4b-d, Fig S3). Observed

382 daily maximum differences in $\delta^2 H_X$ were 18.0‰, 21.0‰, and 25.2‰ for trees, shrubs and herbs

383 respectively (2.8‰, 6.8‰, and 6.5‰ in $\delta^{18}O_X$ in Fig. S4). The expected null model variance

384 was exceeded for each species during its measurement period.

385 Finally, pronounced intra-individual $\delta^2 H_X$ variance was also observed for all monitored

386 firs and beeches in Germany (Fig 4e, Fig. S5). Here, daily maxima differences in $\delta^2 H_X$ were 8.2

387 ‰ and 14.2 ‰ for *Abies alba* and *Fagus sylvatica* respectively (2.0‰ and 4.2 ‰ in $\delta^{18}O_X$ in

388 Fig. S6).

389

390 **3.2. Part B: Model exploration**

391 *Isotope composition of xylem water at stem base and basic model behavior*

392 At the stem base, simulated $\delta^2H_{X,0,t}$ displays a diurnal fluctuation (Fig. 2b, Fig S7) that

393 corresponds to the daily sap flow pattern (Fig. S7). This pattern is caused by shifting diurnal

394 average RWU depth. Early in the morning, when transpiration is low, most of the RWU occurs

395 in deeper layers, where soil matric potential is less negative and where soil water is more

396 depleted in ^2H compared with the soil layers above (Fig. S8a-b). As transpiration increases

397 during the day, a significant proportion of RWU can now be extracted from the drier, shallower

398 layers, where the soil water is enriched in ^2H, i.e., having a higher δ^2H. In the afternoon, as

399 transpiration declines, the isotopic composition reflects again the composition of the more

400 depleted soil water in the deeper soil layers, and it remains constant throughout the night

401 because apart from diffusion SWIFT does not consider mixing of the internal stem water. The

402 mixing effects of diffusion are only noticeable at low sap flow speeds (Fig. 3b).

403   Highest δ^2H_X-values (approx.-59‰) are found in alignment with the diurnal minimum

404 of $\Psi_{X,0,t}$ (approx.-0.85 MPa, Fig. S7). At this moment, the difference between $\Psi_{X,0,t}$ and $\Psi_{S,i,t}$

405 is maximal, enabling water extraction from the upper and driest soil layers. Most root biomass

406 is located near the surface (cf. Jackson *et al.*, 1995; Fig. S8c) and uptake in these layers will

407 result in relatively high contributions to the total RWU.

408   In contrast, differences between $\Psi_{X,0,t}$ and $\Psi_{S,i,t}$ are smaller in the early morning and

409 late afternoon causing root water uptake in the upper soil layers to halt. The decreasing in

410 absolute range of $\Delta\Psi_{i,t}$ translates into higher proportions of RWU originating from deeper, more

411   depleted soil layers. This causes δ^2H_X to drop to a baseline of approx. -67‰. This afternoon

412   depletion of δ^2H_X will henceforth be referred to as the δ^2H_X-baseline drop.

413   *Isotope composition of xylem water at different times, heights and SF_V*

414   Temporal fluctuation in δ^2H_X within a tree at 1.3 m (i.e. the standard sampling height;

415   Analysis A1; Fig. 2a) and other potential sampling heights (e.g. branch collection; Analysis A2;

416   Fig. 2a), are provided in Fig. 2b and 3a. Both analyses show that fluctuations in δ^2H_X depend

417   on the height of measurement and the corresponding time needed to move the water along the

418   xylem conduits. Note that it depends on the selected temporal resolution whether the δ^2H_X-

419   baseline drop at a given height equals the (stem base) minimum (here 1 min, see Fig. S12). In

420   addition to sampling height, analysis A3 depicts the importance of sampling time (Fig. 3a).

421   Outputs of analysis B predict that the occurrence and width of the δ^2H_X-baseline drop are a

422   function of the sap flow velocity SF_V (Fig. 3b). To aid model interpretation and comparability

423   with field data, we (i) provide an illustrative example of normalized δ^2H isotope composition

424   of model-simulated xylem water (β^2H_X) with consideration of extraction error (Fig. 4a), and (ii)

425   display the relation between δ^2H_X variance and cumulative sap flow volumes, for which the

426   piston flow dynamics in SWIFT originate from lateral translation of the δ^2H_X fluctuation at

427    $\delta^2H_{X,0,t}$ (Fig. 2b).

428

3.2.1. Potential biases in average RWU depth estimation

430   Both timing of measurement (Fig. 5a) and SF_V (Fig. 5b) influence average RWU depth

431   estimates derived via the direct inference and end-member mixing analysis method (Fig. S9).

432   Collection of tree samples at 1.30 m can result in erroneous estimation, deviating up to 104 %

433   from the average daily RWU depth (Fig. 5). Plotting the relative error in average RWU depth

434   as a function of time and SF_V (Fig. 5) shows that it is possible to time δ^2H_X measurements in a

435   fashion that captures unbiased estimates of the average RWU depth. Xylem water sampling

436   should be timed to capture the δ^2H_X that corresponds to water extracted at peak RWU, and the

437   expected sampling time can be derived by considering the time needed for the water to reach

438   the point of measurement (i.e. at 1.30 m in Fig. 5).

439

440   **3.2.2. Transport dynamics and sensitivity analysis**

441   Our sensitivity analyses show that the expected absolute error in average RWU depth

442   assessment is directly related to both 1) maximum variance in and 2) the probability of sampling

443   non-representative δ^2H_X values. The maximum variance depends on the height, while the

444   probability of sampling non-representative areas depends on the width of the "δ^2H_X-baseline

445   drop" respectively (defined above). Hence, variation in δ^2H_X is determined by several factors,

446   including the sampling strategy (timing and height of sampling), sap flow velocity (Fig. S10),

447   and below-ground biophysical parameter (Fig. S11). We summarized the most important

448   variables as predicted by SWIFT, which should be considered in subsequent RWU studies.

449   Plants on loamy soils show larger diurnal δ^2H_X variances in comparison with those on clay

450   soils for a similar prevailing isotope gradient across the soil profile. Larger variances

451   correspond to potentially larger errors, but the steeper slope of the δ^2H_X curve results in a thinner

452   δ^2H_X-baseline drop. Hence, loamy soil can result in potentially the large error but this is

453   mediated by a lower probability of sampling non-representative δ^2H_X values during the day.

454   The volume of water taken up by the plant (SF_t; Fig. S11b) affects xylem water potential

455   of the plant at stem base ($\widehat{\Psi}_{X,0,t}$). Higher SF_t requires more negative $\widehat{\Psi}_{X,0,t}$, enabling the plant

456   to access the enriched soil water of more shallow soil layers. Therefore, an increase in SF_t

457   results in the increase of maximum δ^2H_X values (increased maximum error) but also results in

458   a smaller width of the baseline drop (Fig. 2-3). Lower SF_t result in smaller errors, but a larger

459   probability of sampling a non-representative area (Fig. 3b).

460   Root properties, i.e. root membrane permeability (Fig. S11c) strongly influence both the

461   total range of δ^2H_X variance and the width of the δ^2H_X-baseline drops. Decreasing root

462   membrane permeability, but with no alterations to the sap flow volumes, results in thinner δ^2H_X-

463   baseline drops, but higher maximum δ^2H_X variance.

464   In addition, the true sap flow velocity (SF_t per unit of lumen area) will determine the relative

465   importance of diffusion on the δ^2H_X dynamics. Diffusion can cause a smoothing of the peak and

466   a consequent increase in the width of the δ^2H_X-baseline drop. However, as diffusion is

467   proportional to the time that water isotopologues remain in the xylem, its absolute impact on

468   δ^2H_X is negligible in plants with a high true sap flow velocity. In contrast, the impact of diffusion

469   on δ^2H_X dynamics is substantial for plants with very low velocities, where water takes many

470   days to pass from roots to leaves (see supplementary method B).

471   The role of diffusion was investigated using a stepwise ^2H enrichment experiment in Marshall *et al.*

472   (2020) (Fig 6). Analytical solutions of an advection-diffusion equation show that at 0.15 cm, a relatively

473   small diffusivity was required to reproduce the initial increase of xylem isotope signature, with values

474   comparable to these reported for diffusivity of heavy water (Meng *et al.*, 2018). However, at 65 cm, the

475   value of diffusivity required to match the observed initial increase was much higher, suggesting other

476   processes besides molecular diffusivity might contribute to the isotope transport (e.g. variable flow

477   velocities within vessels and among vessels of the xylem network). Note also that the analytical solutions

478   were not able to recover the second part of the curve where the isotope reaches the asymptotic enriched

479   value, which is more gradual in the observations (Fig. 6). This also suggests a complex transport of δ^2H_X

480   in the xylem.

481

482   **4. Discussion**

4.1. Dynamic diurnal isotope compositions of xylem water along plant stems

Empirical field data show pronounced δ_{xyl} variance along the stem length (Fig. 3) and over a sub-daily time period (Fig. 4). Our model explorations suggest that basic plant hydraulic functioning can result in shifting mixtures of δ^2H_X entering the plant (Fig. 2-3). Daily $\Psi_{X,0,t}$ fluctuations interact with the $\Psi_{S,i,t}$ profile causing different parts of the root distribution to be active during the day. The fluctuations in δ^2H_X at the stem base propagate along the xylem with a velocity proportional to the sap flow and this produces variability in sampled δ^2H_X that is much larger than the expected measuring error. Consequently, rather than being static, δ^2H_X values along the height of a plant should be envisioned as a dynamic diurnal process.

Importantly, we show that high variance in δ^2H_X can result in an incorrect assessment of differences in average RWU depths between plants. Differences do not necessarily result from variability in average RWU depth, but may result from monitoring plants at different heights (Fig. 2-3), at different times (Fig. 3a) or by comparing individuals which have different SF_V (Fig. 3b) and xylem anatomical properties. For example, depending on SF$_V$ and lumen area, the isotopic signal can take hours or days to travel from roots to leaves - as was also observed experimentally (Steppe *et al.*, 2010; Magh *et al.*, 2020; Marshall *et al.*, 2020).

Low SF_V allows multiple δ^2H_X-baseline drops over the length of a single tree. Sampled δ^2H_X can reflect soil isotopic composition of the past several days. Our sensitivity analysis reveals that various soil and plant characteristics have an important role in determining both the daily maximum δ^2H_X variance as well as the width of the δ^2H_X -baseline drop. These two characteristics directly impact (i) the expected maximum bias in estimates of average RWU depth and (ii) the chance of measuring δ^2H_X values that do not represent a mixture of all rooting layers during peak RWU (i.e. measurements in the baseline drop). Ultimately, these factors will challenge the use of stable water isotope to study the terrestrial water fluxes as recently

507   reviewed by Penna *et al.* (2018). We additionally advocate that future research should explore

508   the minimum set of (bio)physiological drivers and processes that require quantification to

509   correctly interpret δ^2H_X along the hydraulic pathway length of a plant.

510

511   **4.2. General applicability of model and results**

512   A necessary condition for diurnal shifts in RWU is the existence of water potential differences,

513   e.g. more negative water potentials in the upper layers where trees usually have higher root

514   density, which can cause a disproportional partitioning of diurnal RWU between deep and

515   shallow roots over a diurnal course. The pronounced variance in δ_{xyl} identified in this study is

516   intrinsic to the isotopic tracing technique for RWU assessment, as this method relies on the

517   existence of a soil water isotopic profile. Such profiles are the result of soil evaporation, a

518   process inextricably coupled to water potential heterogeneity, and hence to variance in δ^2H_X.

519   Plant transpiration results from a complex interaction between atmospheric demands

520   (i.e. driven by VPD and radiation) and stomatal conductance that depends on tolerance for

521   drought stress and soil moisture content. We may expect diurnal fluctuation in radiation and

522   VPD, and hence in water transport and depth of water absorption, as modeled here to be a

523   general phenomenon in nature. Moreover, much greater fluctuations in VPD and radiation

524   should be expected under natural conditions than the diurnal cycle described here, and these

525   will increase the variability of transpiration fluxes, leading to even more complex dynamics of

526     $\Psi_{X,0,t}$. Specifically, the model simulations suggest that intra-individual variability of δ^2H_X will

527   reflect the past changes of RWU dynamics, including RWU dynamics driven by changes of

528   environmental demands. For instance, a changing degree in cloud cover that impacts sap flow

529   dynamics can influence $\Psi_{X,0,t}$ rather abruptly (e.g. in lianas; Chen *et al.*, 2015) and lead to

530   instantaneous changes in the δ^2H composition of the water mixture taken up at the root level.

531   This can complicate the comparison of different plants sampled at different heights and times.

532   Note that, based on our model, we expect that soil isotopic enrichment experiments will

533   generate extensive δ^2H_X variation along the length of trees whenever diurnal RWU fluctuations

534   cause water extraction to shift between labeled and unlabeled soil layers. Furthermore, when

535   enrichment experiments target trees with different hydraulic properties (such as SF_V) care

536   should be taken to determine when and where to sample these trees to assess a potential ^2H

537   enrichment in xylem water (Fig. 6, but see Magh *et al.*, 2020;).

538

4.3.   Alternative causes of δ_{xyl} fluctuation

540   The SWIFT model provides a simple traceable and mechanistic explanation, using diurnal

541   variations in SF_t and RWU, for the pronounced variance and dynamic nature of the δ_{xyl}

542   fluctuations with plant height and time of field samples (e.g. Fig. 3-4) and elsewhere (Cooper

543   *et al.* 1991). However, several other processes might contribute to generate variability, while

544   others can act to damp this variability. In the next section, we will discuss alternative causes,

545   complementary and antagonistic, that contribute to the observed intra-individual δ_{xyl} variances.

546   *i.   Fractionation at root or stem level*

547   An increasing body of observations shows the occurrence of isotopic fractionation at the

548   root level governed by root membrane transport (Lin & Sternberg, 1993; Vargas *et al.*, 2017)

549   or by unknown reasons (Zhao *et al.*, 2016). Brinkmann *et al.* (2019) hypothesize that root level

550   fractionation causes disparity when average RWU depth calculations based on δ^2H_X

551   measurements are compared with those of $\delta^{18}O_X$. However, it is difficult to imagine a scenario

552   where root fractionation by itself can explain the observed diurnal fluctuations in δ_{xyl} with

553   height and time. Even if root fractionation significantly contributed to variation in δ_{xyl}, we

554 would still need to take into account diurnal fluctuation in RWU to explain the observed

555 patterns. Isotopic enrichment of xylem water along the stem length was observed in association

556 with stem transpiration (Dawson & Ehleringer, 1993; Barnard *et al.*, 2006). However, this

557 phenomenon is generally restricted to non-suberized plants and in woody branches in close

558 vicinity to the evaporative surface of the plant (Dawson & Ehleringer, 1993). Isotopic

559 enrichment can, therefore, not explain the variances in δ_{xyl} observed in our empirical data, which

560 were sampled within the main stem (data French Guiana) or from lignified branch segment

561 distant from evaporative surfaces (data China and Germany).

562   ii.   *Temporal and spatial soil dynamics*

563   Soil water content can be extremely heterogeneous in the three spatial dimensions as well

564 as in time with complex dynamics of soil water movement. For example, hydraulic lift vertically

565 redistributes soil water through the roots (Dawson & Ehleringer, 1993), which may change the

566 water isotopic composition of the water mixture in the rhizosphere that is taken up by roots.

567 Specifically, hydraulic lift redistributes and mixes the isotopic signal of depleted soil water in

568 deeper layers with the enriched soil water signal in the rhizosphere in shallower layers. This

569 should lead to lower variation in the soil water accessible to the plant, and hence less variation

570 along plant height. Horizontal heterogeneity of water content may also affect δ_{xyl} variance as

571 soil water potentials and the isotope composition of soil water are interlinked. Under these

572 conditions, it is important to understand how much the radial distribution of roots will naturally

573 average out soil heterogeneity. However, note that heterogeneity in the soil does not

574 automatically translate in variability in the xylem. Differential root water uptake driven by the

575 diurnal fluctuation in water potential gradients in the soil-plant interface is still required to

576 generate variability in the xylem isotopic signature.

577   *iii.*   *Storage tissue and phloem enrichment*

578   Storage tissues release water and sugars into the xylem conduits on a daily basis to support

579   water transpiration demand (Goldstein et al., 1998; Morris et al., 2016; Secchi et al., 2017) or

580   to repair embolism (Salleo et al., 2009; Secchi et al., 2017). Both water and sugars are

581   transported in and out of storage tissue via symplastic pathways using plasmodesmata and

582   aquaporins (Knipfer et al., 2016; Secchi et al., 2017), a pathway that has been linked to isotopic

583   fractionation in roots (Ellsworth & Williams, 2007). Moreover, phloem transports

584   photosynthetic assimilates that were produced in the leaves and are therefore potentially

585   affected by transpiration fractionation (Gessler *et al.*, 2013). Hence, these metabolic molecules

586   might show higher values of δ^2H and $\delta^{18}O$ compared to RWU. Water release from storage or

587   phloem tissue might locally alter δ_{xyl} (White et al., 1985). Additionally, the time between water

588   storage and release could bridge multiple days, and corresponding isotopic composition may

589   reflect soil conditions antecedent a dry spell when the isotopic signature of soil was less

590   vertically stratified. It is evident that such dynamics are complex, and it is hard to predict how

591   storage tissue and phloem enrichment affect observed δ_{xyl} patterns. Importantly, xylem isotopic

592   sampling cannot differentiate between water resulting from RWU or storage, and therefore we

593   cannot exclude the possibility that tissue and phloem enrichment play a role. At a minimum this

594   adds further uncertainty to RWU assessment. Water derived from storage tissues might also be

595   present in larger fraction in higher parts of the plants, especially branches, as contamination

596   accumulates as water moves upwards.

597   Unfortunately, to our best knowledge, empirical data on the isotopic composition of storage

598   tissue and its spatiotemporal dynamics are absent in the literature. Future research should target

599   impact assessment of storage water on intra-individual δ_{xyl}, allowing proper implementation in

600   the model.

601   *Diffusion processes*

602   Diffusion is a process of net movement of molecules from a region of higher concentration

603   to a region of lower concentration. Consequently, diffusion dampens δ_{xyl} variability, both in

604   time and space within water xylem. Although the mutual diffusion coefficient of heavy water

605   in normal water is very small and flow within vessels is laminar, other processes might still

606   contribute to generating diffusion along the xylem. For example, as the water moves through

607   the complex network of vessels, differences in velocities between vessels of different sizes

608   cause some particles to move faster or slower than average flow. According to the Hagen–

609   Poiseuille law, the flow in each vessel is proportional to the fourth power of the vessel radius

610   and the mean velocity to the square of the radius, thus potentially generating large differences

611   in particle velocities depending on the vessel size distribution and other anatomical properties.

612   Even within a single vessel, velocity is parabolic with a maximum flow velocity in the center

613   and zero at the vessel walls.

614   **4.4. A way forward**

615   The observed large δ_{xyl} variance and temporal dynamics in the empirical data suggest

616   the need for a critical assessment of the stable isotope tracer technique for RWU studies.

617   However, it also creates new opportunities. Since δ_{xyl} variance and temporal dynamics herein

618   likely relate to various plant physiological processes, monitoring of variation in δ_{xyl} can allow

619   a more integrated understanding of plant water transport and hydraulic properties.

620   Combining a plant hydraulic model with *in situ* SF_V, $\delta^2H_{S,i}$ and $\Psi_{S,i,t}$ can also help

621   improve the robustness of RWU assessment and interpretation. Measurements of $\delta^2H_{S,i}$ and

622      $\Psi_{S,i,t}$ at multiple depths, i.e. by installing soil water suction cups working at a vacuum (i.e.

623   Rennenberg *et al.*, 1996) and multiple soil matric potential sensors that measure at a high

624   temporal frequency, should be especially valuable since the SWIFT model showed high

625   sensitivity to alterations of this variable and these can be directly supplied as model inputs. At

626 the same time, the availability of SF_t measurements allows for identifying the moment when

627 water uptake from all root layers is at its maximum, which can be used to determine the optimal

628 timing of sampling at a given height providing a more robust estimation of average RWU depth

629 and uptake.

630 Alongside the modeling approach presented here, new ways to study δ^2H_X at a high

631 temporal scale are strongly encouraged. For example, the pioneering work of Volkmann *et al.*

632 (2016) to the development of an *in situ* continuous isotope measurement technique that offers

633 the possibility for monitoring δ_{xyl} at a sub-hourly resolution. This technique holds strong

634 promise for further elucidating the natural δ^2H_X variances found within plants and the

635 physiology processes from which these variances result. Such high temporal resolution of

636 isotope measurements, coupled with *in situ* monitoring of various environmental and plant

637 biophysical metrics, are needed for both model improvement and further validation. Moreover,

638 these seem inevitable to eventually differentiate all causal mechanisms of the observed intra-

639 individual δ_{xyl} variance.

640

5. Conclusions

642 A collection of empirical field data show pronounced variance and high temporal

643 fluctuations in δ_{xyl}. Moreover, these high temporal fluctuations in δ_{xyl} emanate from basic plant

644 hydraulic functioning as model explorations show. We expect the observed δ_{xyl} variance and

645 sub-daily fluctuations result, for a large part, from the mechanisms considered here, though

646 various other physiological processes could also affect δ_{xyl}.

647 Our theoretical explorations warn that variability in the isotope composition of plant

648 xylem water can result in erroneous average RWU depth estimation and will complicate the

649 interpretation and comparison of data: samples taken at different heights, times or plants

differing in SF_V may incorrectly show differences in average RWU depth. We further predict that various soil parameters and plant hydraulic parameters affect (i) the absolute size of the error and (ii) the probability of measuring δ_{xyl} values that do not represent the well-mixed values during the plants' peak RWU. Hydraulic models, such as SWIFT, could help to design more robust sampling regimes that enable improved comparisons between studied plants. We advocate the addition of SF_t, which indirectly reflects diurnal RWU fluctuations, and $\Psi_{S,i,t}$ monitoring as a minimum in future RWU assessments since these parameters were predicted to be the predominant factors introducing variance in δ_{xyl} from the SWIFT model exploration. However, soil texture and root permeability are also key measurements especially when comparing across species and sites.

Our findings do not exclude additional factors that impact the observed intra-individual δ_{xyl} variance and temporal fluctuation as many processes can act simultaneously and are not mutually exclusive. Therefore, we strongly emphasize the need for more research. Directed studies that validate and quantify the relative impact of other plant physiological processes towards variance in δ_{xyl} are a prerequisite before improved modeling tools can be developed.

Acknowledgment

This research was funded by the European Research Council Starting Grant 637643 (TREECLIMBERS), the FWO grants (1507818N, V401018N to HDD), the Carbon Mitigation Initiative at Princeton University (MD, MDV), Agence Nationale de la Recherche "Investissement d'Avenir" grant (CEBA: ANR-10-LABX-25-01), the Belgian American Educational Foundation (BAEF to FM) and the WBI (FM). LW acknowledges partial support from the Division of Earth Sciences of National Science Foundation (EAR-1554894). We are grateful to Samuel Bodé, Megan Bartlett, Isabel Martinez Cano, and Pedro Hervé-Fernández

674 who provided feedback on analytical and interpretative aspects of the study. We thank Dries

675 Van Der Heyden, Wim Van Nunen, Laurence Stalmans, Oscar Vercleyen, Katja Van Nieuland,

676 Stijn Vandevoorde, and Clément Stahl for data collection and lab processing. We credit Pascal

677 Petronelli and Bruce Hoffman for species identification, and Cora N. Betsinger for

678 proofreading. Cheng-Wei Huang's work provided inspiration for this research.

679

680 **Author contribution**

681 H.V., M.D.V, and P.B. supervised and provided guidance throughout all aspects of the research.

682 H.D.D., M.D.V, and H.V. designed the study. H.D.D., K.K., R.K.M., J.D.M., L.W., and L.Z.

683 collected and processed the empirical datasets. The model was developed and coded by H.D.D,

684 M.D.V, M.D., and F.M. All authors contributed to the interpretation of the results and the text

685 of the manuscript.

686

687 **Data availability**

688 Both the French Guiana data and the SWIFT model are available on the GitHub repository

689 HannesDeDeurwaerder/SWIFT. For the availability of the data collected in China and

690 Germany, readers are referred to Zhao *et al.* (2014) and Magh *et al.* (2020), respectively.

691

692 **Competing interests**

693 The authors declare that they have no conflict of interest.

694

References

Araguás-Araguás L, Froehlich K, Rozanski K. **1998**. Stable isotope composition of precipitation over southeast Asia. *Journal of Geophysical Research: Atmospheres* **103**: 28721–28742.

Azzalini A. **2013**. *The skew-normal and related families*. Cambridge University Press.

Barbeta A, Gimeno TE, Clavé L, Fréjaville B, Jones SP, Delvigne C, Wingate L, Ogée J. **2020**. An explanation for the isotopic offset between soil and stem water in a temperate tree species. *New Phytologist*.

Barnard RL, De Bello F, Gilgen AK, Buchmann N. **2006**. The δ18O of root crown water best reflects source water δ18O in different types of herbaceous species, Rapid Commun. Mass Sp., 20, 3799–3802.

Brinkmann N, Eugster W, Buchmann N, Kahmen A. **2019**. Species-specific differences in water uptake depth of mature temperate trees vary with water availability in the soil. *Plant Biology* **21**: 71–81.

Čermák J, Ulrich R, Staněk Z, Koller J, Aubrecht L. **2006**. Electrical measurement of tree root absorbing surfaces by the earth impedance method: 2. Verification based on allometric relationships and root severing experiments. *Tree physiology* **26**: 1113–1121.

Cernusak LA, Farquhar GD, Pate JS. **2005**. Environmental and physiological controls over oxygen and carbon isotope composition of Tasmanian blue gum, Eucalyptus globulus. *Tree physiology* **25**: 129–146.

Chen Y, Cao K, Schnitzer SA, Fan Z, Zhang J, Bongers F, Chen Y. **2015**. Water-use advantage for lianas over trees in tropical seasonal forests. : 128–136.

Clapp RB, Hornberger GM. **1978**. Empirical equations for some soil hydraulic properties. *Water resources research* **14**: 601–604.

Cooper LW, DeNiro MJ, Keeley JE. **1991**. The relationship between stable oxygen and hydrogen isotope ratios of water in astomatal plants.

Dawson TE, Ehleringer JR. **1991**. Streamside trees that do not use stream water. *Nature* **350**: 335–337.

Dawson TE, Ehleringer JR. **1993**. Isotopic enrichment of water in the "woody" tissues of plants: implications for plant water source, water uptake, and other studies which use the stable isotopic composition of cellulose. *Geochimica et Cosmochimica Acta* **57**: 3487–3492.

Dawson TE, Mambelli S, Plamboeck AH, Templer PH, Tu KP. **2002**. Stable isotopes in plant ecology. *Annual review of ecology and systematics* **33**: 507–559.

De Deurwaerder H, Hervé-Fernández P, Stahl C, Burban B, Petronelli P, Hoffman B, Bonal D, Boeckx P, Verbeeck H. **2018**. Liana and tree below-ground water competition—evidence for water resource partitioning during the dry season. *Tree Physiology*.

Doussan C, Pierret A, Garrigues E, Pagès L. **2006**. Water uptake by plant roots: II–modelling of water transfer in the soil root-system with explicit account of flow within the root system–comparison with experiments. *Plant and soil* **283**: 99–117.

Ehleringer JR, Dawson TE. **1992**. Water uptake by plants: perspectives from stable isotope

composition. *Plant, Cell & Environment* **15**: 1073–1082.

Ellsworth PZ, Williams DG. **2007**. Hydrogen isotope fractionation during water uptake by woody xerophytes. *Plant and Soil* **291**: 93–107.

Epila J, Maes WH, Verbeeck H, Camp J Van, Okullo JBL, Steppe K. **2017**. Plant measurements on African tropical Maesopsis eminii seedlings contradict pioneering water use behaviour. *Environmental and Experimental Botany* **135**: 27–37.

Früh T, Kurth W. **1999**. The hydraulic system of trees: theoretical framework and numerical simulation. *Journal of theoretical Biology* **201**: 251–270.

Gessler A, Brandes E, Keitel C, Boda S, Kayler ZE, Granier A, Barbour M, Farquhar GD, Treydte K. **2013**. The oxygen isotope enrichment of leaf-exported assimilates–does it always reflect lamina leaf water enrichment? *New Phytologist* **200**: 144–157.

Goldsmith GR, Muñoz-Villers LE, Holwerda F, McDonnell JJ, Asbjornsen H, Dawson TE. **2012**. Stable isotopes reveal linkages among ecohydrological processes in a seasonally dry tropical montane cloud forest. *Ecohydrology* **5**: 779–790.

Goldstein G, Andrade JL, Meinzer FC, Holbrook NM, Cavelier J, Jackson P, Celis A. **1998**. Stem water storage and diurnal patterns of water use in tropical forest canopy trees. *Plant, Cell & Environment* **21**: 397–406.

Hervé-Fernández P, Oyarzún C, Brumbt C, Huygens D, Bodé S, Verhoest NEC, Boeckx P. **2016**. Assessing the 'two water worlds' hypothesis and water sources for native and exotic evergreen species in south-central Chile. *Hydrological Processes* **30**: 4227–4241.

Huang C, Domec J, Ward EJ, Duman T, Manoli G, Parolari AJ, Katul GG. **2017**. The effect of plant water storage on water fluxes within the coupled soil–plant system. *New Phytologist* **213**: 1093–1106.

Jackson PC, Cavelier J, Goldstein G, Meunzer FC, Holbrook NM. **1995**. Partitioning of water-resources among plants of a lowland tropical forest. *Oecologia* **101**: 197–203.

De Jong van Lier Q, Van Dam JC, Metselaar K, De Jong R, Duijnisveld WHM. **2008**. Macroscopic root water uptake distribution using a matric flux potential approach. *Vadose Zone Journal* **7**: 1065–1078.

Knipfer T, Cuneo I, Brodersen C, McElrone AJ. **2016**. In-situ visualization of the dynamics in xylem embolism formation and removal in the absence of root pressure: a study on excised grapevine stems. *Plant Physiology*: pp-00136.

Lanning M, Wang L, Benson M, Zhang Q, Novick KA. **2020**. Canopy isotopic investigation reveals different water uptake dynamics of maples and oaks. *Phytochemistry* **175**: 112389.

Lin G, Sternberg L. **1993**. Hydrogen isotopic fractionation by plant roots during water uptake in coastal wetland plants. Stable isotopes and plant carbon-water relations. Elsevier, 497–510.

Magh R-K, Eiferle C, Burzlaff T, Dannenmann M, Rennenberg H, Dubbert M. **2020**. Competition for water rather than facilitation in mixed beech-fir forests after drying-wetting cycle. *Journal of Hydrology*: 124944.

Mamonov AB, Coalson RD, Zeidel ML, Mathai JC. **2007**. Water and deuterium oxide

permeability through aquaporin 1: MD predictions and experimental verification. *The Journal of general physiology* **130**: 111–116.

Marshall JD, Cuntz M, Beyer M, Dubbert M, Kuehnhammer K. **2020**. Borehole equilibration: testing a new method to monitor the isotopic composition of tree xylem water in situ. *Frontiers in Plant Science* **11**: 358.

Meinzer FC, Andrade JL, Goldstein G, Holbrook NM, Cavelier J, Wright SJ. **1999**. Partitioning of soil water among canopy trees in a seasonally dry tropical forest. *Oecologia* **121**: 293–301.

Meißner M, Köhler M, Schwendenmann L, Hölscher D. **2012**. Partitioning of soil water among canopy trees during a soil desiccation period in a temperate mixed forest. *Biogeosciences* **9**: 3465–3474.

Meng W, Xia Y, Chen Y, Pu X. **2018**. Measuring the mutual diffusion coefficient of heavy water in normal water using a double liquid-core cylindrical lens. *Scientific reports* **8**: 1–7.

Meunier F, Rothfuss Y, Bariac T, Biron P, Richard P, Durand J-L, Couvreur V, Vanderborght J, Javaux M. **2017**. Measuring and modeling hydraulic lift of Lolium multiflorum using stable water isotopes. *Vadose Zone Journal*.

Morris H, Plavcová L, Cvecko P, Fichtler E, Gillingham MAF, Martínez-Cabrera HI, McGlinn DJ, Wheeler E, Zheng J, Ziemińska K. **2016**. A global analysis of parenchyma tissue fractions in secondary xylem of seed plants. *New Phytologist* **209**: 1553–1565.

Muñoz-Villers LE, Geris J, Alvarado-Barrientos S, Holwerda F, Dawson TE. **2019**. Coffee and shade trees show complementary use of soil water in a traditional agroforestry ecosystem. *Hydrology and Earth System Sciences Discussion*.

Orlowski N, Frede HG, Brüggemann N, Breuer L. **2013**. Validation and application of a cryogenic vacuum extraction system for soil and plant water extraction for isotope analysis. *J. Sens. Sens. Syst* **2**: 179–193.

Penna D, Hopp L, Scandellari F, Allen ST, Benettin P, Beyer M, Geris J, Klaus J, Marshall JD, Schwendenmann L. **2018**. Ideas and perspectives: Tracing terrestrial ecosystem water fluxes using hydrogen and oxygen stable isotopes–challenges and opportunities from an interdisciplinary perspective. *Biogeosciences*.

Phillips DL, Gregg JW. **2003**. Source partitioning using stable isotopes: coping with too many sources. *Oecologia* **136**: 261–269.

Rennenberg H, Schneider S, Weber P. **1996**. Analysis of uptake and allocation of nitrogen and sulphur compounds by trees in the field. *Journal of Experimental Botany* **47**: 1491–1498.

Rothfuss Y, Javaux M. **2017**. Reviews and syntheses: Isotopic approaches to quantify root water uptake: a review and comparison of methods. *Biogeosciences* **14**: 2199.

Salleo S, Trifilò P, Esposito S, Nardini A, Gullo MA Lo. **2009**. Starch-to-sugar conversion in wood parenchyma of field-growing Laurus nobilis plants: a component of the signal pathway for embolism repair? *Functional Plant Biology* **36**: 815–825.

Scholander PF. **1966**. The role of solvent pressure in osmotic systems. *Proceedings of the National Academy of Sciences of the United States of America* **55**: 1407.

Secchi F, Pagliarani C, Zwieniecki MA. **2017**. The functional role of xylem parenchyma cells and aquaporins during recovery from severe water stress. *Plant, cell & environment* **40**:

818 858–871.

819 **Steppe K, Lemeur R**. **2004**. An experimental system for analysis of the dynamic sap-flow
820 characteristics in young trees: results of a beech tree. *Functional Plant Biology* **31**: 83–92.

821 **Steppe K, De Pauw DJW, Doody TM, Teskey RO**. **2010**. A comparison of sap flux density
822 using thermal dissipation, heat pulse velocity and heat field deformation methods.
823 *Agricultural and Forest Meteorology* **150**: 1046–1056.

824 **Vargas AI, Schaffer B, Yuhong L, Sternberg L da SL**. **2017**. Testing plant use of mobile
825 vs immobile soil water sources using stable isotope experiments. *New Phytologist* **215**: 582–
826 594.

827 **Vogel T, Dohnal M, Dusek J, Votrubova J, Tesar M**. **2013**. Macroscopic modeling of plant
828 water uptake in a forest stand involving root-mediated soil water redistribution. *Vadose Zone*
829 *Journal* **12**.

830 **Volkmann THM, Kühnhammer K, Herbstritt B, Gessler A, Weiler M**. **2016**. A method
831 for in situ monitoring of the isotope composition of tree xylem water using laser spectroscopy.
832 *Plant, cell & environment* **39**: 2055–2063.

833 **Walker CD, Richardson SB**. **1991**. The use of stable isotopes of water in characterizing the
834 source of water in vegetation. *Chemical Geology* **94**: 145–158.

835 **Wershaw RL, Friedman I, Heller SJ, Frank PA**. **1966**. Hydrogen isotopic fractionation of
836 water passing through trees. *Advances in organic geochemistry*: 55.

837 **White JWC, Cook ER, Lawrence JR, Broecker WS**. **1985**. The D/H ratios of sap in trees -
838 implications for water sources and tree-ring D/H ratios. *Geochimica et Cosmochimica Acta*
839 **49**: 237–246.

840 **De Wispelaere L, Bodé S, Hervé-Fernández P, Hemp A, Verschuren D, Boeckx P**. **2016**.
841 Plant water resource partitioning and xylem-leaf deuterium enrichment in a seasonally dry
842 tropical climate. *Biogeosciences Discuss.* **2016**: 1–26.

843 **Yakir D**. **1992**. Variations in the natural abundance of oxygen-18 and deuterium in plant
844 carbohydrates. *Plant, Cell & Environment* **15**: 1005–1020.

845 **Yang Q, Xiao H, Zhao L, Zhou M, Li C, Cao S**. **2010**. Stable isotope techniques in plant
846 water sources: a review. *Sciences in Cold and Arid Regions* **2**: 112–122.

847 **Zhao L, Wang L, Cernusak LA, Liu X, Xiao H, Zhou M, Zhang S**. **2016**. Significant
848 difference in hydrogen isotope composition between xylem and tissue water in Populus
849 euphratica. *Plant, Cell & Environment* **39**: 1848–1857.

850 **Zhao L, Wang L, Liu X, Xiao H, Ruan Y, Zhou M**. **2014**. The patterns and implications of
851 diurnal variations in the d-excess of plant water, shallow soil water and air moisture. *Hydrol.*
852 *Earth Syst. Sci.* **18**: 4129–4151.

853 **Zhao L, Xiao H, Zhou J, Wang L, Cheng G, Zhou M, Yin L, McCabe MF**. **2011**. Detailed
854 assessment of isotope ratio infrared spectroscopy and isotope ratio mass spectrometry for the
855 stable isotope analysis of plant and soil waters. *Rapid Communications in Mass Spectrometry*
856 **25**: 3071–3082.

857 **Zimmermann U, Ehhalt D, Münnich K**. **1967**. Soil-Water movement and
858 evapotranspiration: changes in the isotopic composition of the water. Conference on Isotopes
859 in Hydrology. Vienna, 567-585.

860

Tables

 Table 1. Nomenclature.

Symbol	Description	Unit
$A_{R,i}$	The absorptive root area distribution over soil layer i	m^2
A_{Rtot}	The plants' total active fine root surface area	m^2
$A_{SAPWOOD}$	Sapwood area	m^2
A_x	Total lumen area	m^2
b	Shape parameter for the soil hydraulic properties (Clapp & Hornberger, 1978)	dimensionless
B_i	The overall root length density distribution per unit of soil, not necessarily limited to the focal plant.	$m\ m^{-3}$
$\delta^2 H_{X,0,t}$	Isotope composition of plant xylem water at stem base at time t	in ‰ VSMOW
$\delta^2 H_{X,h,t}$	Isotope composition of plant xylem water at height h and time t	in ‰ VSMOW
$\delta^2 H_{S,i}$	Isotope composition of soil water of the ith soil layer (constant over time)	in ‰ VSMOW
δ_{sample}	Isotope composition of water within a sample	in ‰ VSMOW
$\Delta \widehat{\Psi}_{i,t}$	Estimated water potential gradient between stem base and the ith soil layer at time t derived from Eq. (8)	m
$\Delta \Psi_{i,t}$	Soil matric potential gradient between soil and roots at the ith soil layer at time t	$m\ H_2O$
$\beta^2 H_X; \beta^{18} O_X$	Normalized isotope composition of plant xylem water	in ‰ VSMOW
$f_{i,t}$	The fraction of water taken up in the ith soil layer at time t	dimensionless
h	Measurement height	m
i	Soil layer index	dimensionless
δ_{xyl}	Isotope composition of plant xylem water	in ‰ VSMOW
k_i	Soil-root conductance of the ith soil layer	s^{-1}
K_{max}	Maximum soil hydraulic conductivity	$m\ s^{-1}$
k_R	Effective root radial conductivity	s^{-1}
k_S	The conductance associated with the radial water flow between the soil and the root surface	s^{-1}
$K_{S,i}$	Soil hydraulic conductivity at the ith soil layer	$m\ s^{-1}$
ℓ	The approximated radial pathway length of water flow between bulk soil and root surface	m
LF	Lumen fraction per unit sapwood area	$m^2\ m^{-2}$
n	Number of unique contributing water sources	#
Ψ_{sat}	Soil matric potential at soil saturation	m
$\Psi_{S,i,t}$	Soil matric potential of the ith soil layer at time t	m
$\Psi_{X,0,t}$	Water potential at the base of the plant stem at time t	m
R	Heavy to light isotope ratio measured in the sample or standard	%

$RWU_{i,t}$	Net amount of water entering and leaving the root tissues per unit of time in the ith soil layer at time t	$m^3\ s^{-1}$
SF_t	Instantaneous sap flow at time t	$m^3\ s^{-1}$
SF_S	Sap flow velocity, calculated as the sap flow per sapwood area	$m\ h^{-1}$
SF_V	True sap flux density, calculated as the sap flow per lumen area	$m\ h^{-1}$
τ	Delay before the isotope composition of xylem water at stem base reaches stem height h	s
θ_{sat}	Soil moisture content at soil saturation	$m^3\ m^{-3}$
$\theta_{S,i,t}$	Soil moisture content of the ith soil layer at time t	$m^3\ m^{-3}$
z_i	Soil depth of the ith soil layer	m

863

864

Figures
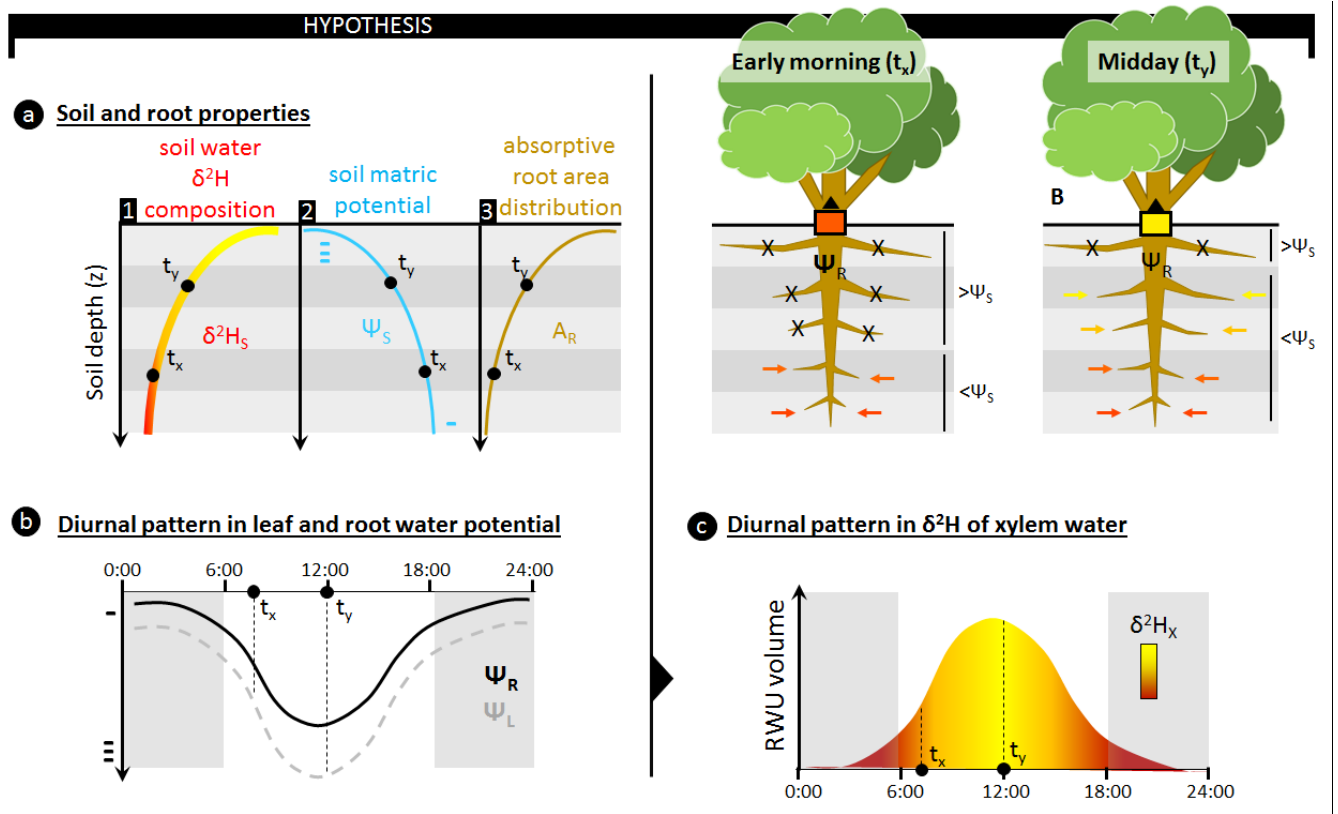
Fig 1. The use of stable water isotopes (δ^2H and $\delta^{18}O$) to assess the relative depth of root water

uptake (RWU) requires a depth gradient in isotopic composition of soil water (δ^2H_S) to be

present (**a, line 1**), as only then can the relative contribution of different soil layers to the

isotopic composition in a plant's xylem water (δ^2H_X) be derived. These δ^2H_S gradients occur

naturally as the result of evaporative soil drying during drought conditions, however, these

conditions also result in the formation of a gradient in soil matric potential (Ψ_S), ensuring an

increasing Ψ_S with depth (**a, line 2**). RWU and sap flow in plants are passive processes where

water flows in the direction of decreasing water potentials. Specifically for RWU, this implies

that water influx through the absorptive root area (A_R; **a, line 3**) of a plant's root is facilitated

whenever the water potential in the root (Ψ_R) is more negative than the surrounding Ψ_S. As A_R

and Ψ_S are generally not uniform with soil depth (z), the relative contribution of a specific soil

layer to RWU will depend on (i) the difference between Ψ_S and Ψ_R in that soil layer, and (ii)

the relative amount of absorptive root area in that soil layer. Stable water isotopes techniques

881   assume that the δ^2H$_X$ reflects the contribution of δ^2H_S from all soil layers. However, this does

882   not account for diurnal fluctuations in Ψ_R which are invoked by the diurnal patterns in a plant's

883   transpiratory water demands (**panel b**). Typically, more negative Ψ_R values are observed when

884   water demands are high, i.e. around midday. However, a decrease in Ψ_R will result in higher

885   RWU, and alter the contribution of different soil layers to RWU. Specifically, dryer and

886   shallower soil layers, with more negative Ψ_S, could start contributing to RWU as Ψ_R decreases

887   (**panel c**). For example, in the early morning (situation t_x) when Ψ_R is high, only deeper soil

888   layers where $\Psi_S > \Psi_R$ contribute to overall δ^2H composition of the RWU flux. As Ψ_L and Ψ_R

889   decrease towards midday (situation t_y) more water can be absorbed from shallower soil layers.

890   As the A_R in these shallow soil layers is high, they strongly affect the relative contribution of

891   δ^2H_S entering the plant. Hence, diurnal fluctuations in Ψ_R will result in fluctuating mixtures of

892   δ^2H_S entering the plant. As these δ^2H_S mixtures are transported along the xylem pathway, they

893   produce variance in δ^2H_X, which could complicate RWU assessments via stable water isotope

894   analysis.
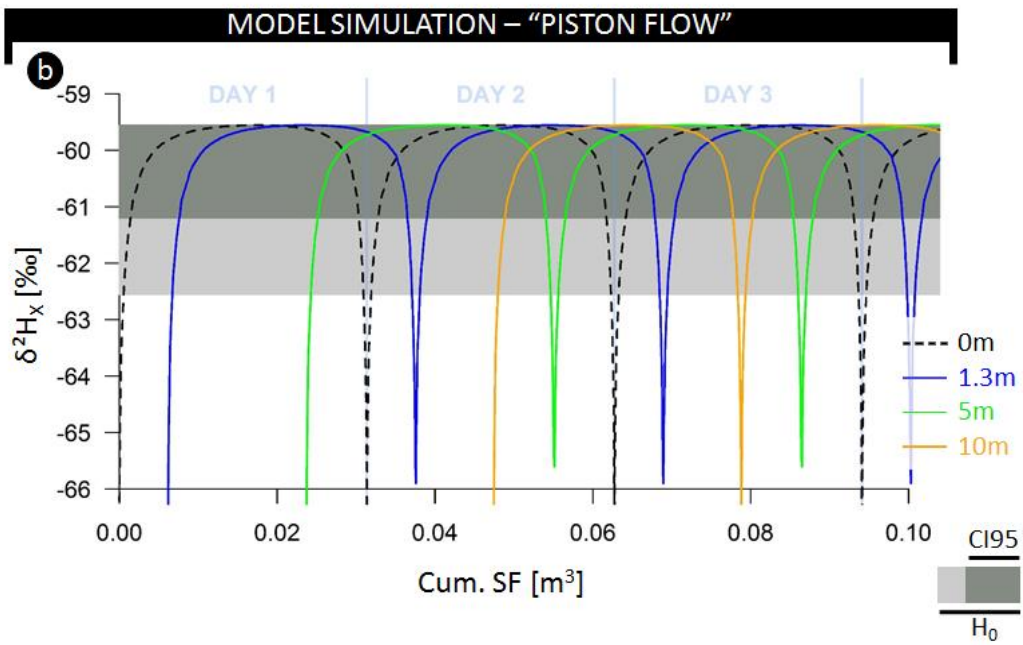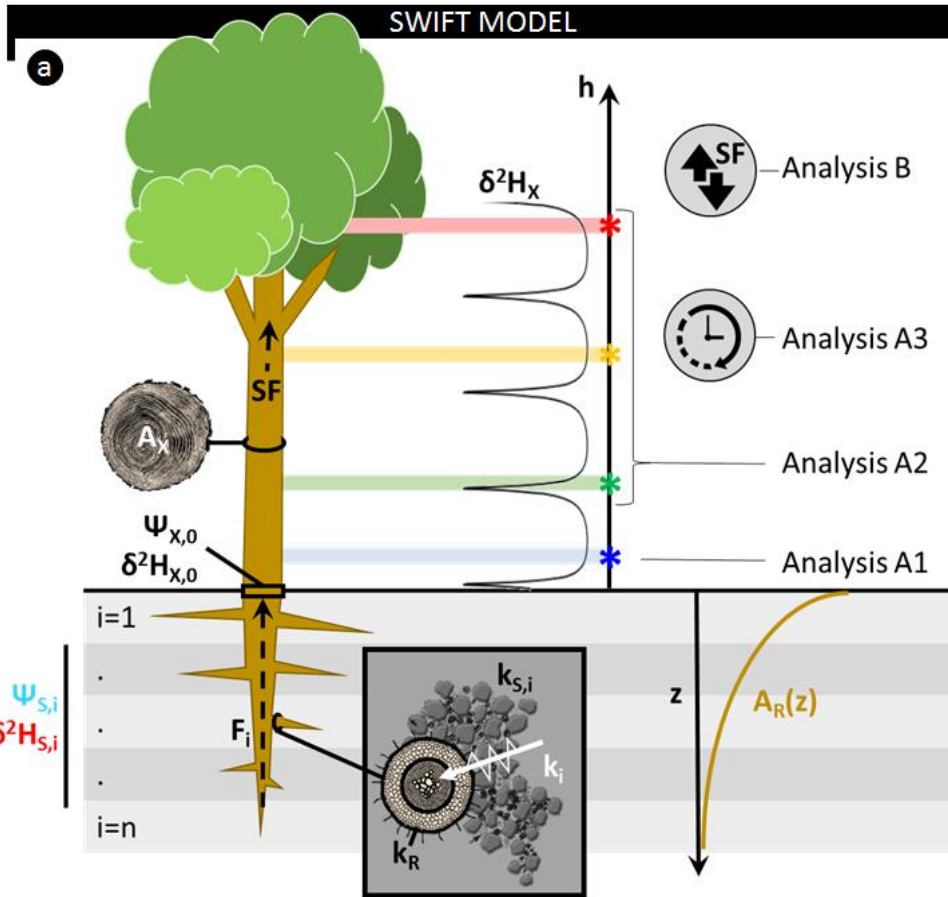
897 **Fig. 2. (a)** Schematic representation of the model and considered analysis detailed in the text.

898 **(b)** Simulated fluctuations in δ^2H composition of plant xylem water as a function of the

899 cumulative sap flow volume measured at various heights: stem base (0 m, black dashed), 1.3 m

900 (blue), 5 m (green) and 10 m (red). The horizontal grey colored envelope delineates the

901 acceptable variance from the stem mean according to the null model (H_0), i.e. assuming no

902 variance along the length of a lignified plant aside from potential extraction error (i.e. 3‰).

903 Herein, the dark grey envelope indicates the confidence interval comprising 95% of potential

904 extraction error (CI95).

905
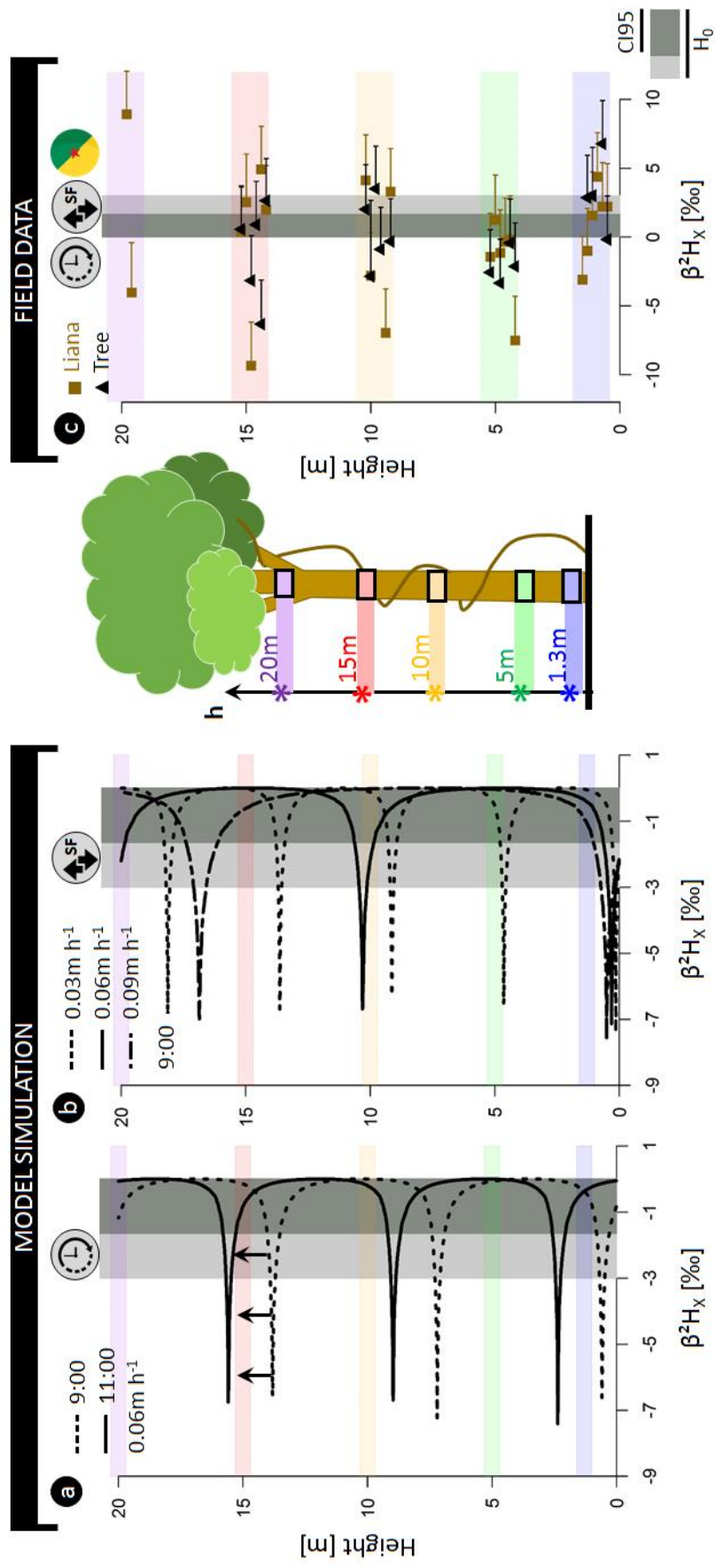
Fig 3. (a) Model outputs for model analysis A3 representing the normalized δ^2H composition of xylem water (β^2H$_X$) as a function of the tree height simulated for different sampling times (9:00 and 11:00). The modeled tree has an average daily sap flux density of 0.06 m h^{-1} (SF$_S$; ~ daily true sap flux density $SF_V = 0.42$ m h^{-1}). **(b)** Model outputs for model analysis B where β^2H$_X$ in relation to stem height is shown at 9:00 a.m., but parameterized with distinct SF_S, i.e. 0.09, 0.06 and 0.03 m h^{-1} (corresponding to SF_V of 0.64, 0.42 and 0.19 m h^{-1}, respectively). The standard parameterization used for both study analysis is detailed in Table S1. **(c)** Field measurements of β^2H$_X$ for six lianas (■) and six trees (▲). Error whiskers are the combination of potential extraction and measurement errors of the isotope analyzer. A species-specific breakdown of the field data is provided in Fig S2. The horizontal grey colored envelope in all panels delineates the acceptable variance from the stem mean according to the null model (H$_0$), i.e. assuming no variance along the length of a lignified plant aside from potential extraction error (i.e. 3‰). Herein, the dark grey envelope indicates the confidence interval comprising 95% of potential extraction error (CI95).
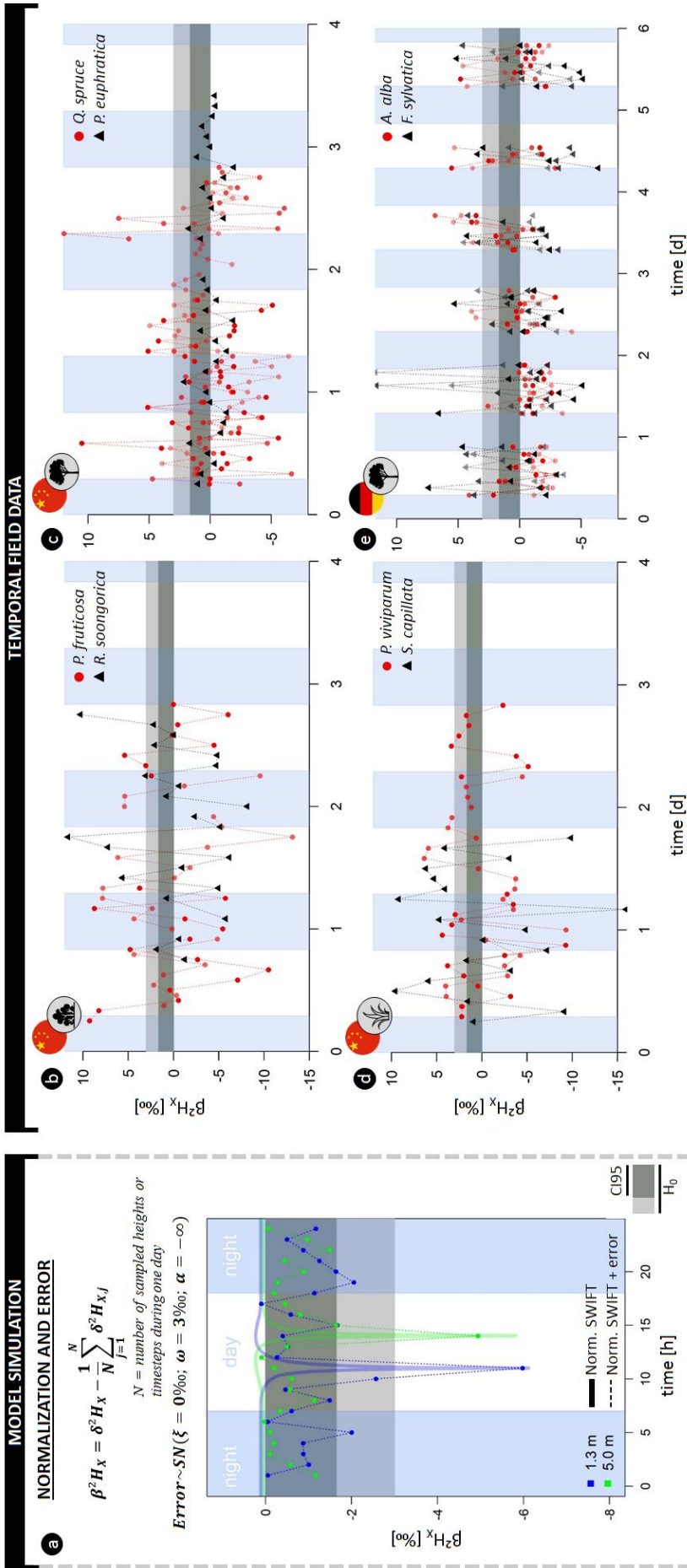
924 **Fig 4. (a)** Illustrative example of model simulations transformed in normalized δ^2H composition

925 of xylem water (β^2H$_X$) at 1.3 (blue) and 5m (green) sampling height, with the formula provided.

926 Thicker lines indicate model simulations without error, line connected dots indicate a scenario

927 of hourly sampling with consideration of extraction error (i.e. a negative skew-normal

928 distribution; ξ = 0‰, the scale ω = 3‰, and shape α = -∞). **(b-e)** High temporal field

929 measurements of β^2H_X of (b) two shrubs, (c) two trees, and (d) two herb species sampled in the

930 Heihe River Basin (northwestern China); and (e) two tree species sampled in the "Freiamt"

931 field site in south-west Germany. The horizontal grey colored envelope in all panels delineates

932 the acceptable variance from the stem mean according to the null model (H$_0$), i.e. assuming no

933 variance along the length of a lignified plant aside from potential extraction error (i.e. 3‰).

934 Herein, the dark grey envelope indicates the confidence interval comprising 95% of potential

935 extraction error (CI95). A breakdown of the field data on species and individual level is

936 provided in the supplementary figures (Fig S3-S4-S5-S6)

937

938

939
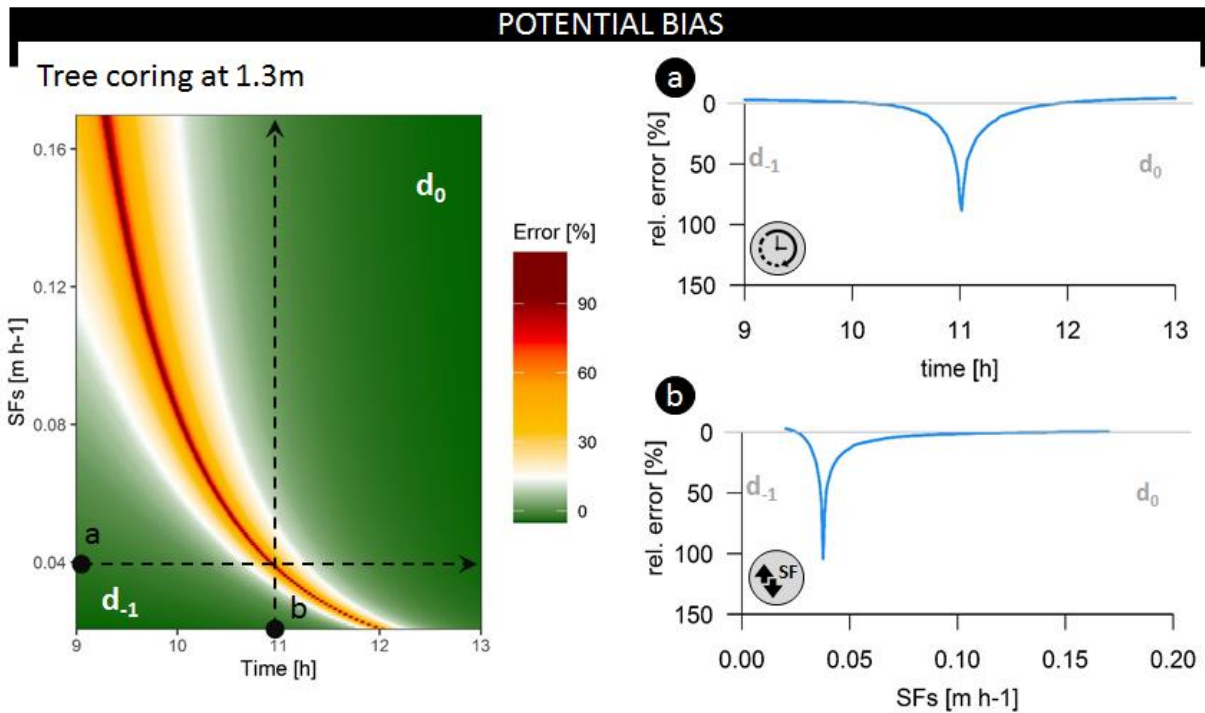
Fig 5. Relative error on the inferred average root water uptake depth (i.e. bias between the average daily and the instantaneous derived average RWU depth) at coring height of 1.3m, throughout the common sampling period (9:00 until 13:00) and over a range of potential SF_S (in m h^{-1}) – corresponding to SF_V range of 0.15–1.25 m h^{-1}. Both dotted lines describe test scenarios evaluated in the breakup panels. The dynamics in relative error when sampling **(a)** over different time steps, restricting sap flux density at 0.04 m h^{-1} (i.e. $SF_V = 0.28$ m h^{-1}), or **(b)** over different SF_S-values when restricting sampling time at 11 am. d_{-1} and d_0 indicate whether the derived average RWU depth error corresponds to the previous or current day of measurement.

949
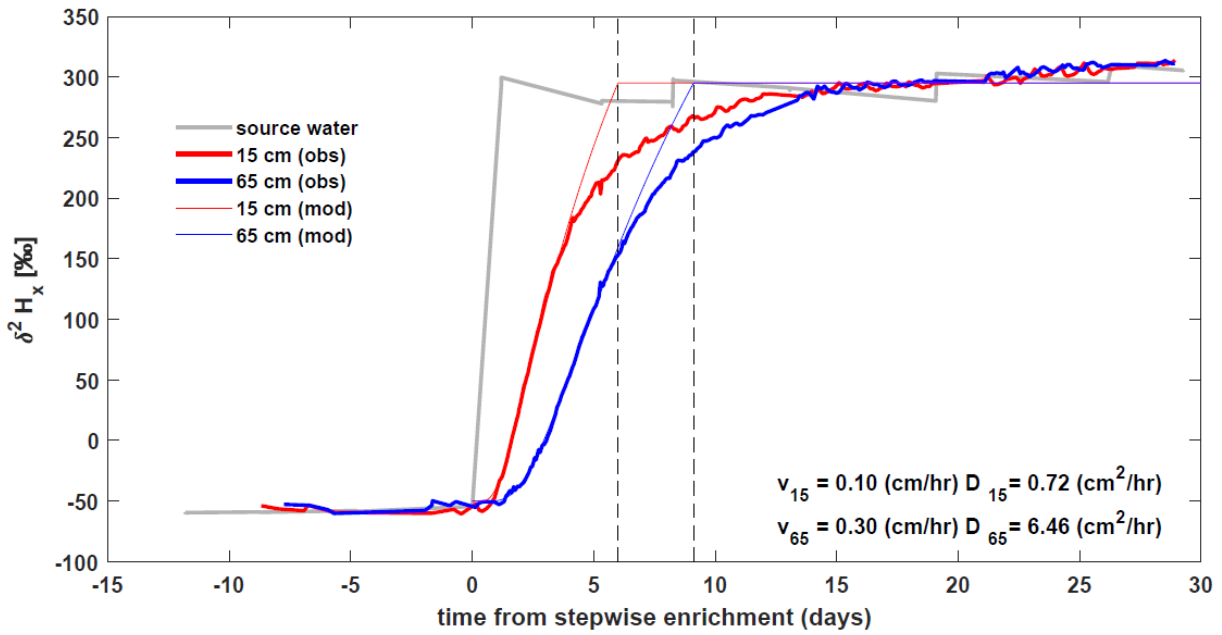
Fig. 6. Basic model validation, comparing continuous *in situ* δ^2H_X measurements of a stepwise

^2H enrichment experiment (Marshall *et al.,* 2020) with analytical solutions of advection-

diffusion equation, at heights 0.15m (—) and 0.65m (—) on a pine tree (*Pinus pinea L*). The

source water of the intact-root, isotopic enrichment greenhouse experiment, is presented in

grey. Model parameters, velocity, and diffusion were fitted by visual inspection independently

for the two heights to match the initial increase in isotope signature (values reported in the

bottom right)